

Article

# Substitution Effects in Spin-Polarized $(\text{Cr}_{4-x}\text{Fe}_x)_{0.5}\text{AC}$ (A = Ge, Si, Al) MAX Phases

Natalja A. Fedorova<sup>1,2</sup>, Alena V. Kovaleva<sup>1</sup>, Julia S. Olshevskaya<sup>3</sup>, Daria A. Ivanova<sup>1</sup>, Victoria V. Kozak<sup>1,2</sup>, Alexander A. Shubin<sup>2</sup> , Anton S. Tarasov<sup>1,2</sup> , Sergey N. Varnakov<sup>1</sup>, Sergei G. Ovchinnikov<sup>1,2</sup> , Evgeniya M. Moshkina<sup>1</sup> , Olga A. Maximova<sup>1,2</sup>, Pavel V. Avramov<sup>3,\*</sup>  and Felix N. Tomilin<sup>1,2,\*</sup> 

<sup>1</sup> Kirensky Institute of Physics, Federal Research Center KSC SB RAS, 660036 Krasnoyarsk, Russia; a1enka.k.3009000@gmail.com (A.V.K.); taras@iph.krasn.ru (A.S.T.); maximo.a@mail.ru (O.A.M.)

<sup>2</sup> Department of Physical and Inorganic Chemistry, Siberian Federal University, 660041 Krasnoyarsk, Russia

<sup>3</sup> Department of Chemistry, College of Natural Sciences, Kyungpook National University, 80 Daehak-ro, Buk-gu, Daegu 41566, Republic of Korea; julia665102.o@gmail.com

\* Correspondence: paul.veniaminovich@knu.ac.kr (P.V.A.); felixnt@gmail.com (F.N.T.)

**Abstract:** The use of spintronic devices with a tunable magnetic order on small scales is highly important for novel applications. The MAX phases containing transition metals and/or magnetic ion-substituted lattices attract a lot of attention. In this study, the magnetic and electronic properties of  $(\text{Cr}_{4-x}\text{Fe}_x)_{0.5}\text{AC}$  (A = Ge, Si, Al) compounds were predicted and investigated within the density functional theory. It was established that single-substituted  $(\text{Cr}_3\text{Fe}_1)_{0.5}\text{AC}$  (A = Ge, Si, Al) lattices are favorable in terms of energy. An analysis of the magnetic states of the MAX phases demonstrated that their spin order changes upon substitution of iron atoms for chromium ones. It was found that mostly the  $(\text{Cr}_{4-x}\text{Fe}_x)_{0.5}\text{GeC}$  and  $(\text{Cr}_{4-x}\text{Fe}_x)_{0.5}\text{AlC}$  lattices acquire a ferrimagnetic state in contrast to  $(\text{Cr}_{4-x}\text{Fe}_x)_{0.5}\text{SiC}$  for which the ferromagnetic spin order dominates. It was pointed out that the atomic substitution could be an efficient way to tune the magnetic properties of proposed  $(\text{Cr}_{4-x}\text{Fe}_x)_{0.5}\text{AC}$  (A = Ge, Si, Al) MAX phases.

**Keywords:** MAX phase; density functional theory; B3LYP; spintronics; magnetic properties; electronic properties



**Citation:** Fedorova, N.A.; Kovaleva, A.V.; Olshevskaya, J.S.; Ivanova, D.A.; Kozak, V.V.; Shubin, A.A.; Tarasov, A.S.; Varnakov, S.N.; Ovchinnikov, S.G.; Moshkina, E.M.; et al.

Substitution Effects in Spin-Polarized  $(\text{Cr}_{4-x}\text{Fe}_x)_{0.5}\text{AC}$  (A = Ge, Si, Al) MAX Phases. *Magnetochemistry* **2023**, *9*, 147. <https://doi.org/10.3390/magnetochemistry9060147>

Academic Editor: Carlos J. Gómez García

Received: 21 April 2023

Revised: 19 May 2023

Accepted: 26 May 2023

Published: 30 May 2023



**Copyright:** © 2023 by the authors. Licensee MDPI, Basel, Switzerland. This article is an open access article distributed under the terms and conditions of the Creative Commons Attribution (CC BY) license (<https://creativecommons.org/licenses/by/4.0/>).

## 1. Introduction

The MAX phases form a family of layered ternary compounds with the formal stoichiometry  $M_{n+1}AX_n$  ( $n = 1, 2, 3 \dots$ ), where  $M$  element is a transition metal,  $A$  is a  $p$  element (Si, Ge, Al, S, Sn, etc.), and  $X$  is carbon or nitrogen [1]. The MAX phases exhibit the unique physical properties that are typical for both metals and ceramics. They have a high electrical and thermal conductivity with respect to metals, are easy to manufacture, and are highly thermal shock-resistant. Simultaneously, they are characterized by stiffness, light weight, remarkable oxidation, and wear resistance of ceramics. Therefore, it is no wonder that the MAX phases have attracted close attention of researchers [1–5].

With the onrush in the advanced industrial technology sectors, it becomes highly promising to seek the MAX phases with desired magnetic and electronic properties in order to expand the range of their application in spintronics, magnetocalorics, computer and space technology, etc. [6]. Taking into account a vast variety of elements that can be used to synthesize the MAX phases, as well as the complexity of this synthesis, the experimental verification of the behavior and properties of synthesized compounds under specific conditions becomes impractical. For this reason, the quantum chemical modeling of different MAX phases, and their minimization and prediction of electronic and spin properties is of a crucial importance.

MAX phases are good candidates for spintronics for several reasons. First, MAX phases belong to a family of quasi-2D materials which possess some unique intrinsic properties

different from other materials such as “classical” semiconductors and metals. Second, MAX phases are considered metals and, consequently, a source of spin current, which makes them different from magnetic semiconductors. They can be used in spintronics as a ferromagnetic layer or simple metal layer. The hexagonal symmetry and laminate structure of MAX phases brings unusual electronic properties and, as a result, exceptional macroscopic physical properties. For example, the band structure of many MAX phases exhibits distinctive Dirac cones in ARPES experimental spectra [7]. This feature in the band structure provides the possibility of the existence of massless fermions that can be used for developing electronic devices based on relativistic effects [8]. The hexagonal lattice allows the creation of hybrid multilayer structures combining MAX phases and other hexagonal 2D materials such as graphene, nitrides, chalcogenides, and laminate topological insulators that may be used in future 2D spintronics. Another important advantage of MAX phases is their extreme thermal, mechanical, and chemical resistance, which can make them suitable for some applications with extreme conditions [9].

Currently, keen interest is focused on studying magnetic MAX phases. The thermodynamic stability and electronic and magnetic properties of MAX phases have been exploited using quantum-chemical modeling [10–15]. However, the effect of partial replacement of M elements by *d* metals remains poorly understood. The few magnetic MAX compounds that have been synthesized to date exhibit outstanding properties attractive for both fundamental research and advanced applications. The properties include complex magnetism in the bulk rare-earth  $(\text{Mo}_{2/3}\text{Re}_{1/3})_2\text{AlC}$  *i*-MAX phases [16] and magnetic  $(\text{Cr,Mn})_2\text{GaC}$  thin films [17,18], as well as the large uniaxial magnetostriction in the nanolaminated  $\text{Mn}_2\text{GaC}$  phase [5,19,20].

The atomic and electronic structure of parent  $\text{Cr}_2\text{GeC}$  MAX phase was examined theoretically following its experimental synthesis by Nowotny [21] in 1971 and several contemporary works [9,20,21]. Nevertheless, the magnetic properties and the effect of substitution by metal atoms have not yet been studied using theoretical approaches. The  $\text{Cr}_2\text{AlC}$  MAX phase synthesis was reported in Refs. [22,23]. So far, its partner, the  $\text{Fe}_2\text{AlC}$  MAX phase has not been synthesized but following theoretical predictions [22,23] it may exhibit challenging atomic and electronic structure and magnetic and chemical properties.

In this study, the atomic and electronic structure and spin states of a number of  $(\text{Cr}_{4-x}\text{Fe}_x)_{0.5}\text{AC}$  MAX phases with  $\text{M} = \text{Cr}$ ,  $\text{A} = \text{Al}$ ,  $\text{Si}$ , and  $\text{Ge}$ , and  $\text{X} = \text{C}$ , were comprehensively investigated using ab initio PBC DFT calculations coupled with Gaussian-type basis sets. The chromium centers in the lattices were steadily and consequently substituted by iron ions since they possess close atomic and ionic radii (Table S1) and display similar ferromagnetic spin ordering in most compounds. For the sake of comparison, parent  $\text{Cr}_2\text{GeC}$  lattice was examined using density functional theory (DFT) [24–26] within a set of generalized gradient approximation (GGA) [27], meta-GGA, GGA + U [28], and Heyd–Scuseria–Ernzerh (HSE06) DFT approaches [29]. Special attention was paid to a systematic search of iron-doped  $\text{Cr}_2\text{GeC}$ ,  $\text{Cr}_2\text{SiC}$ , and  $\text{Cr}_2\text{AlC}$  MAX phases promising for advanced spin-related applications. Based on extensive electronic structure calculations, it was shown that substitution of even a minor amount of chromium ions by iron can drastically change the magnetic properties of parent MAX phases.

## 2. Computational Details

The atomic and electronic structure and spin states of a number of regular 3D crystal lattices of  $(\text{Cr}_{4-x}\text{Fe}_x)_{0.5}\text{AC}$  MAX phases with  $\text{M} = \text{Cr}$ ,  $\text{A} = \text{Al}$ ,  $\text{Si}$ , and  $\text{Ge}$ , and  $\text{X} = \text{C}$  was studied in reciprocal space via the ab initio DFT approach using GGA Perdew–Burke–Ernzerhof (PBE) [27], hybrid exchange–correlation PBE0-13 [30], B3LYP [31,32], and meta-GGA M06 [33], M062 [33], and M06L [34] functionals coupled with the *pob*-DZVP-*rev2* basis set [35]. For the sake of comparison, parent  $\text{Cr}_2\text{SiC}$  (Figure 1, right image) and  $\text{Fe-CrSiC}$  (Figure 1, left image) lattices were considered to investigate the effects of structural ion swaps. The  $\text{Fe}_x\text{Cr}_{4-x}\text{SiC}$  lattice was generated by replacement of two outer layers of chromium ions by iron ones (image I, II and III in Figure 1). At both PBE and M06L levels of

theory (Figure S1), the  $a$  and  $b$  unit cell structural parameters coincide well with theoretical values for  $\text{Cr}_2\text{SiC}$  [36] and  $\text{Fe}_2\text{SiC}$  [37] phases. At the same time, the  $c$  parameter was determined using all functionals but M062 are close to the data published in Refs. [36,37]. The deviations of the iron and chromium atomic charges from the corresponding values [36,37] are almost identical (Figure S2) with the maximum one no larger than unity.

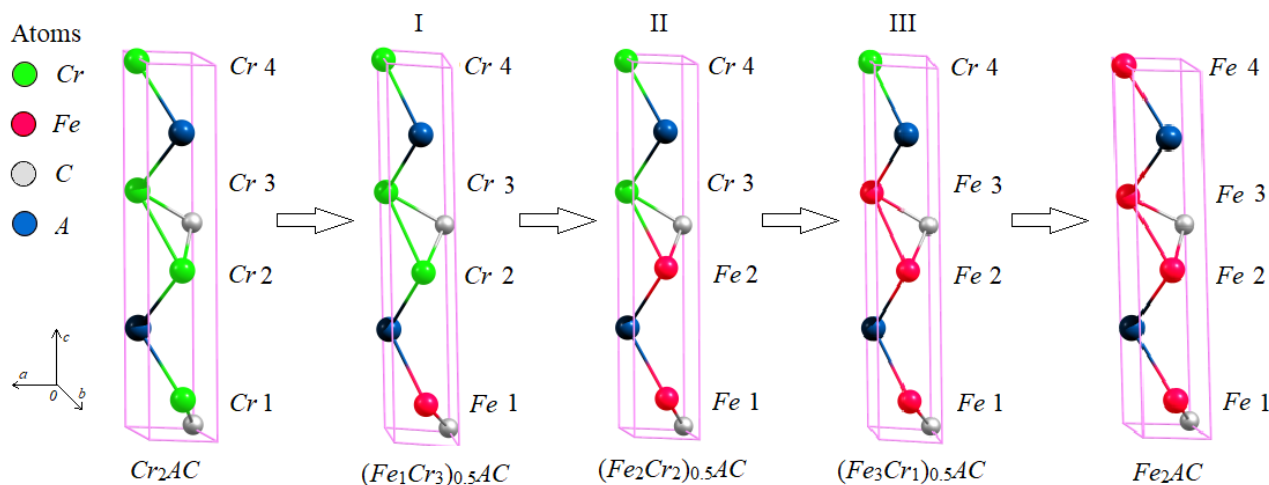


**Figure 1.** Stepwise substitution of Cr ions by Fe ones in parent  $\text{Cr}_2\text{AC}$  ( $A = \text{Ge, Si, Al}$ ) lattices. Cr ions are depicted in green, Fe ions are depicted in red, carbon atoms in grey, and A elements ( $\text{Ge, Si, Al}$ ) are depicted in blue. Explanation of figures I, II and III given in the text.

Comparison of the unit cell parameters (Figure S1) shows that PBE0-13, B3LYP, and M06 functionals yield comparable results, while the values obtained using the PBE and M062 functionals are different. In particular, at the M06L level of theory the  $a$  and  $b$  parameters are lower and the  $c$  value is comparable to the data found via PBE0-13, B3LYP, and M06 functionals. Moreover, PBE and M062 functionals yield different partial charge distribution (Figure S2). When comparing the magnetic moments localized at iron and chromium ions, one can see (Figure S3) that PBE0-13, B3LYP, and M06 functionals show similar results, whereas at PBE and M06L levels of theory the magnetic moments are low with the highest values obtained via the M062 functional. Comparing theoretical results, one can see that for electronic structure calculations of  $(\text{Cr}_{4-x}\text{Fe}_x)_{0.5}\text{AC}$  MAX phases the PBE0-13, B3LYP, and M06 functionals provide the best results. It is well known that for the light elements with  $Z \leq 36$  B3LYP DFT functional band structures coincide well with both experimental and theoretical data [38,39], so a hybrid exchange-correlation B3LYP functional was chosen to run electronic structure calculations.

All B3LYP/*pob*-DZVP-*rev2* electronic structure calculations of  $(\text{Cr}_{4-x}\text{Fe}_x)_{0.5}\text{AC}$  MAX phases were carried out using CRYSTAL 17 software [40]. The cutoff limits for Coulomb and exchange series which arise in the self-consistent field (SCF) equation for periodic systems were set at  $10^{-7}$  a.u. for the Coulomb overlap, Coulomb penetration, exchange overlap, and exchange pseudo-overlap in the direct space and at  $10^{-14}$  a.u. for exchange pseudo-overlap in reciprocal space. The SCF convergence condition was set at  $10^{-6}$  a.u. from the total energy difference between two successive cycles [41]. The shrinkage factors of Monkhorst-Pack [42] and Gilat [43] meshes had the same value (the SHRINK parameter was set to 8). The atomic coordinate gradients were estimated analytically. The equilibrium structure was determined via the quasi-Newtonian approach with the Broyden–Fletcher–Goldfarb–Shanno algorithm using the Hessian matrix update scheme [44]. The parameters of the unit cell and all atomic coordinates were fully optimized.

The  $(\text{Cr}_{4-x}\text{Fe}_x)_{0.5}\text{AC}$  ( $A = \text{Ge, Si, Al}$ ) MAX phases have  $P6_3/mmc$  (194) hexagonal unit cells with  $a$  and  $c$  parameters specified in Refs. [30,37,38] with the unit cells designed by replacement of chromium ions by one, two, or three iron atoms successively with dramatic reduction in the unit cell symmetry up to space group  $C_1$  (1) [45,46]. To describe the

electronic characteristics of each single  $(\text{Cr}_{4-x}\text{Fe}_x)_{0.5}\text{AC}$  MAX phase, the band structures were calculated bypassing high-symmetry points of the first Brillouin zone of the hexagonal lattice (Figure S4) [34,39].

To identify the most stable lattices, the binding energies of all  $(\text{Cr}_{4-x}\text{Fe}_x)_{0.5}\text{AC}$  MAX phases were calculated according to Equation (1),

$$E_{\text{Bond}} = E_{(\text{Cr}_{4-x}\text{Fe}_x)_{0.5}\text{AC}}^{\text{tot}} - (4-x)E_{\text{Cr}} - xE_{\text{Fe}} - 2E_{\text{A}} - 2E_{\text{C}}, \quad (1)$$

with Fe substitution energies determined according to Equation (2),

$$\Delta E_{\text{Sub}} = E_{\text{Cr}_2\text{AC}}^{\text{tot}} - E_{(\text{Cr}_{4-x}\text{Fe}_x)_{0.5}\text{AC}}^{\text{tot}} + xE_{\text{Fe}} - xE_{\text{Cr}} \quad (2)$$

where  $E_{(\text{Cr}_{4-x}\text{Fe}_x)_{0.5}\text{AC}}^{\text{tot}}$  is the total energy of the substituted lattice,  $E_{\text{Cr}_2\text{AC}}^{\text{tot}}$  is the total energy of parent  $\text{Cr}_2\text{AC}$ ,  $E_{\text{Cr}}$ ,  $E_{\text{Fe}}$ ,  $E_{\text{A}}$ , and  $E_{\text{C}}$  are the energies of free-standing Cr, Fe, A (Ge, Si, Al), and C atoms, respectively, and  $4-x$  and  $x$  are stoichiometric coefficients of Cr and Fe ions, respectively, with  $x$  substituted Cr ions.

To simulate the magnetic properties, spin-polarized electronic structure calculations were carried out for unit cells consisting of four M (either Cr or Fe) ions, two A (Ge, Si, or Al), and two carbon atoms with the alternation of the directions along the  $c$  axis of magnetic moments localized at  $d$  elements. All possible spin states—ferromagnetic (FM- $n$ ), ferrimagnetic (FiM- $n$ ), and antiferromagnetic (AFM- $n$ )—formed in  $(\text{Cr}_{4-x}\text{Fe}_x)_{0.5}\text{AC}$  MAX phases were considered (Table S2) in the study with ferrimagnetic and antiferromagnetic ones specified by alternating the magnetic moments localized at the ions.

### 3. Results and Discussion

#### 3.1. The Atomic Structure of Substituted MAX Phases

The stepwise substitution of one, two, three, and four Cr ions by Fe ones in different positions with consequent formation of  $(\text{Cr}_{4-x}\text{Fe}_x)_{0.5}\text{GeC}$  ( $x = 1-4$ ) lattices (Figure 1). In the type-I substitution, a Fe ion is localized either at the first, second, third, or fourth site, producing in fact four different lattices. The type-II substitution includes six structures with two Fe ions in sites 1-2, 3-4; 1-3, 2-4; and 1-4, 2-3. The type-III substitution includes four lattices resembling type-I. It is necessary to note that the substitution of Cr ions in  $(\text{Cr}_{4-x}\text{Fe}_x)_{0.5}\text{AC}$  ( $\text{A} = \text{Si}, \text{Al}$ ) lattices produces analogous structures.

Binding energies  $E_{\text{Bond}}$ , substitution energies  $\Delta E_{\text{Sub}}$ , and cell volumes and densities directly demonstrate a decrease in  $a$  and  $c$  lattice parameters upon substitution (Figure 2a,b) with  $a$  and  $c$  parameters decreased by  $0.12 \text{ \AA}$  (4%) and  $0.79 \text{ \AA}$  (6%), respectively. At the iron content of 0% ( $\text{Cr}_2\text{GeC}$ ), the volume is  $102.20 \text{ \AA}^3$ /unit cell and at 100% concentration ( $\text{Fe}_2\text{GeC}$ ) it is equal to  $88.48 \text{ \AA}^3$ , which corresponds to a decrease in the lattice parameters by 13%. It could be caused by the differences in Cr and Fe ionic radii, bond lengths and angles. Fe substitution of Cr ions in parent  $\text{Cr}_2\text{AC}$  causes the changes of atomic charges and the absolute values and directions of the ionic magnetic moments.

As the iron content increases from  $\text{Cr}_2\text{SiC}$  to  $\text{Fe}_2\text{SiC}$ , the  $a$  unit cell parameter changes by no more than 7% (Figure 2a,b) with volume equal to  $97.97 \text{ \AA}^3$  for  $\text{Cr}_2\text{Si}$  and  $81.74 \text{ \AA}^3$  for  $\text{Fe}_2\text{SiC}$ , which corresponds to a drop in the lattice parameter of 16%. In addition, the change in the unit cell volume is affected by a combination of the ratio between the chromium and iron ionic radii and the differences in the length of Cr–Si and Fe–Si bonds.

Upon consequent substitution of Cr ions by Fe ones in the  $\text{Cr}_2\text{AlC}$  lattice, the  $a$  parameter steadily decreases; however, for the terminal  $\text{Fe}_2\text{AlC}$  compound, the parameter sharply grows by  $0.07 \text{ \AA}$  relative to the value of the parent  $\text{Cr}_2\text{AlC}$ . Lattice parameter  $c$  decreases gradually with the  $\text{Cr}_2\text{AlC}$ -to- $\text{Fe}_2\text{AlC}$  transition by  $0.68 \text{ \AA}$ . At an iron content of 0% ( $\text{Cr}_2\text{AlC}$ ), the volume is  $89.20 \text{ \AA}^3$  and for 100% ( $\text{Fe}_2\text{AlC}$ ), it is  $83.8 \text{ \AA}^3$ , which corresponds to a decrease of 6%. The change in the crystal lattice parameters leads to a decrease in the lattice volume and a consequent increase in the density. The  $\text{Cr}_2\text{AlC}$  MAX phase

shows a weaker change in the atomic structure as compared with the  $\text{Cr}_2\text{GeC}$  and  $\text{Cr}_2\text{SiC}$  MAX phases.

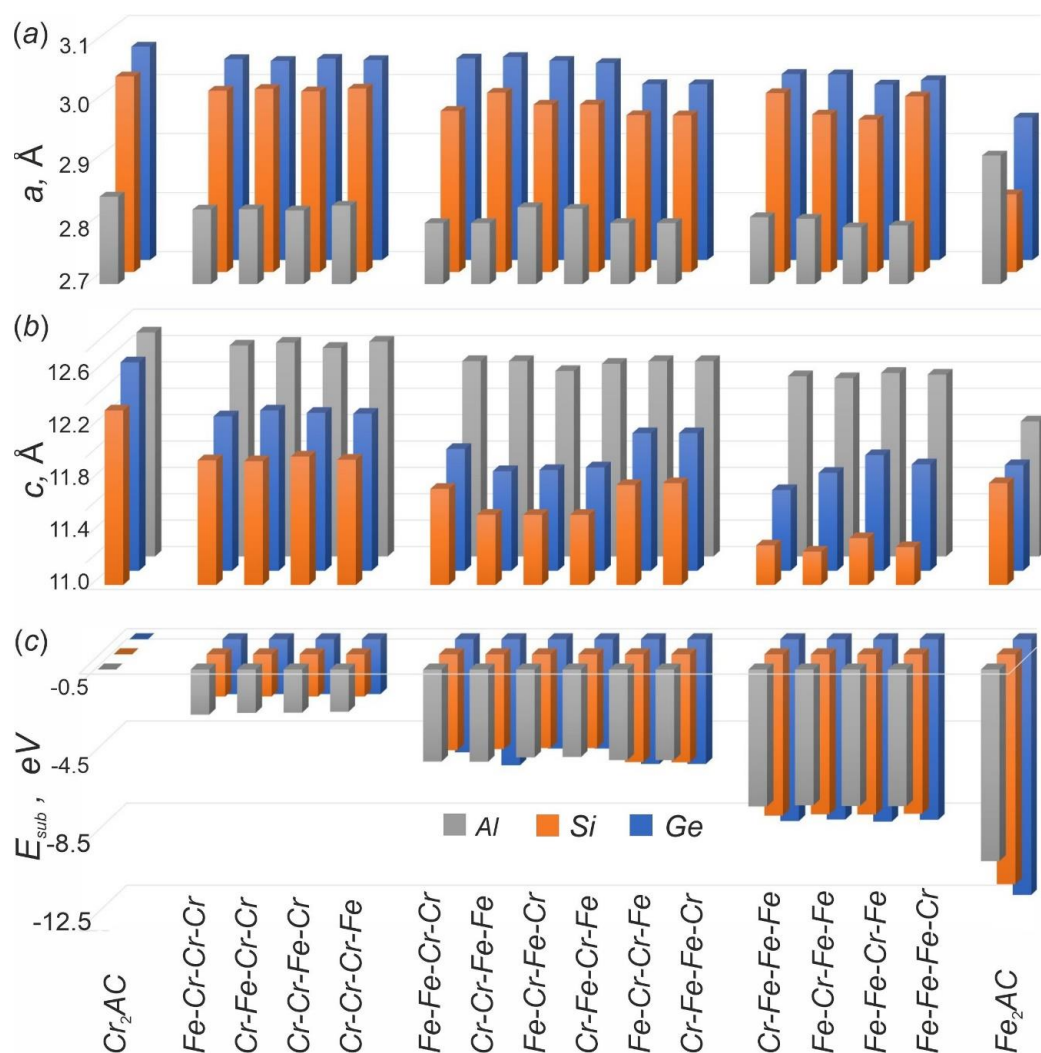


**Figure 2.** Changes in crystal lattice parameters  $a$  and  $c$  and substitution energies of  $(\text{Cr}_{4-x}\text{Fe}_x)_{0.5}\text{AC}$  ( $A = \text{Ge}, \text{Si}, \text{Al}$ ) in ferromagnetic state upon substitution. (a) Change of  $(\text{Cr}_{4-x}\text{Fe}_x)_{0.5}\text{AC}$  crystal lattice parameter  $a$  upon substitution. (b) Change of  $(\text{Cr}_{4-x}\text{Fe}_x)_{0.5}\text{AC}$   $c$  parameter. (c) Change of  $(\text{Cr}_{4-x}\text{Fe}_x)_{0.5}\text{AC}$  substitution energies. Atoms are presented in the order of their positioning in the cell. Blue histograms correspond to the phases with  $A = \text{Ge}$ ; terracotta histograms represent  $A = \text{Si}$ ; and gray indicates  $A = \text{Al}$ .

### 3.2. Energetic Characteristics

At the transition from  $\text{Cr}_2\text{AC}$  to  $\text{Fe}_2\text{AC}$ , the binding energy drops (Figure S5), which in turn affects the substitution energy. It should be noted (Figure 2c) that the change in the substitution energy is almost independent of the arrangement of substituted atoms. The growth of the binding and substitution energies during the gradual transition from chromium to iron demonstrates the complexity of iron substitution and explains the fact that the iron-containing MAX phases have not yet been obtained. For example, the  $\text{Cr}_2\text{GeC}$  MAX phase was synthesized [9,20,21], while all attempts to obtain the  $\text{Fe}_2\text{GeC}$  MAX phase failed. As can be seen (Figures 2c and S5), the lattices that are favorable with respect to energy are single-substituted like  $(\text{Cr}_3\text{Fe}_1)_{0.5}\text{AC}$  ( $A = \text{Ge}, \text{Si}, \text{Al}$ ). This is confirmed by the experimental data reported by Pazniak [12,47], which showed the achievement of the iron solubility maximum up to 3.4 at % which corresponds to the  $(\text{Cr}_{0.932}\text{Fe}_{0.068})_2\text{AlC}$

compound. This concentration of iron was obtained in a film synthesized via pulsed laser deposition. It cannot be denied that a concentration close to  $(\text{Cr}_3\text{Fe}_1)_{0.5}\text{AC}$  studied in this work can be obtained using another A component and synthetic methods such as magnetron sputtering [6]. Taking this into account, the structures with one metal ion replaced were further examined.

### 3.3. Band Structure

To analyze the electronic properties, the band structures are displayed in Figure 3. A detailed description of the band anisotropy around highly symmetrical points [48] can be found in Figure S3. Since the density of states at the Fermi level turns out to be non-zero, it can be said that all considered compounds have a metallic conductivity typical of most MAX phases, which in turn confirms the consistency of the calculated data and correctness of the choice of the functional. The different densities of spin-up ( $\alpha$ ) and spin-down ( $\beta$ ) electrons on the top of the valence band and at the bottom of the conduction band are indicative of the spin polarization of carriers and consequently suggest the possibility of using these compositions in spintronics as a source of spin current in lateral ferromagnet/semiconductor or ferromagnet/graphene (Gr) and vertical ferromagnet/insulator/ferromagnet spin-valve-type nanostructures based on 2D materials. As an example, one can suppose structures that contain semiconducting chalcogenides (Hal) [49] such as MAX/Hal and graphene (Gr) [50,51] such as MAX/Gr or MAX/Gr/MAX.

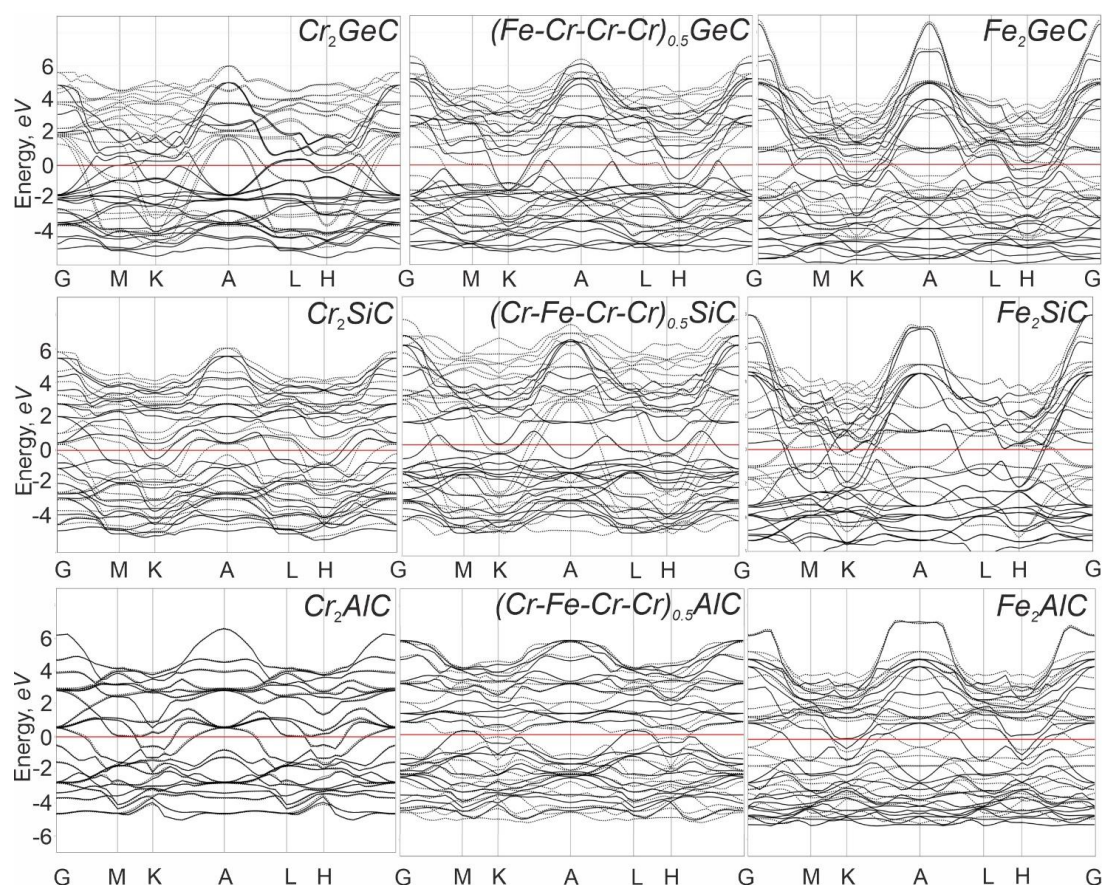


**Figure 3.** Band structures of  $\text{Cr}_2\text{AC}$ ,  $(\text{Fe-Cr-Cr-Cr})_{0.5}\text{AC}$ , and  $\text{Fe}_2\text{AC}$  ( $\text{A} = \text{Ge, Si, Al}$ ) lattices. The red line marks the Fermi levels, black solid lines correspond to the energy levels of  $\alpha$  electrons, and black dotted lines represent the energy levels of  $\beta$  electrons, respectively. The energetically favorable lattices are FM  $\text{Cr}_2\text{GeC}$ , FiM  $\text{Fe}_1\text{Cr}_3\text{GeC}$ , and FiM  $\text{Fe}_2\text{GeC}$  in the germanium-based MAX phases; FiM  $\text{Cr}_2\text{SiC}$ , FM  $\text{Fe}_1\text{Cr}_3\text{SiC}$ , and FM  $\text{Fe}_2\text{SiC}$  in the silicon-based MAX phases; and FiM  $\text{Cr}_2\text{AlC}$ , AFM-6 (FiM)  $\text{Fe}_1\text{Cr}_3\text{AlC}$ , and FiM  $\text{Fe}_2\text{AlC}$  for the aluminum-based MAX phases.

Structural transformation of  $\text{Cr}_2\text{GeC}$  lattice to  $\text{Fe}_2\text{GeC}$  caused by substitution of Cr ions by Fe ones causes gradual manifestation of van Hove singularities (so-called Mexican hat) [52] at A point of Brillouin zone (Figure 3), which implies high density of states (DOS) at the Fermi level and makes the  $\text{Fe}_2\text{GeC}$  MAX phase a good 1D conductor. The electron density in some directions of the reciprocal space of the  $\text{Fe}_2\text{GeC}$  MAX phase reaches its maxima and even under a low applied voltage the electrons at Mexican hat edges may simultaneously tunnel to neighboring regions, which may induce significant anisotropy in the electrical and thermal conductivity, which is very typical for the MAX phases. Similar properties of the conductivity were discovered experimentally for  $(\text{Mn}_{0.5}\text{Cr}_{0.5})_2\text{GaC}$  thin film [53]. In the A direction of the  $\text{Cr}_2\text{GeC}$  band structure, a band gap of about 4 eV is observed, which is indicative of the anisotropy of the electronic properties. The electron and hole bands contribute differently to the conductivity in different directions. Therefore, the  $\text{Cr}_2\text{GeC}$  compound can be attributed to the materials with pronounced carrier-type anisotropy for which positive carriers (holes) are responsible for transport properties within the basal  $xy$  plane and negative carriers (electrons) are responsible for those along the vertical  $z$  axis [54]. At the same time, this anisotropy can be responsible for the magnetic anisotropy observed experimentally [55]. In the  $\text{Fe}_2\text{GeC}$  structure, this feature is less pronounced.

Following the structural transformation from  $\text{Cr}_2\text{SiC}$  to  $\text{Fe}_2\text{SiC}$ , the band gap broadens to 2 eV along the A direction and like for germanium-based MAX phases the Mexican hat gradually appears as well. In contrast to the germanium- and silicon-based MAX phases,  $\text{Cr}_2\text{AlC}$  demonstrates the Dirac cone at the A point of the Brillouin zone (Figure 3), which should determine the main transport properties of the phase. Some topological features of the  $\text{Cr}_2\text{AlC}$  band structure including band inversions that lead to the existence of many crossings and topological nodes were observed both theoretically and experimentally [7]. In addition, at the  $\text{Cr}_2\text{AlC}$ -to- $\text{Fe}_2\text{AlC}$  transition, the  $\alpha$  and  $\beta$  electron densities converge, indicating a decrease in the polarizability of the material. The intermediate  $(\text{Fe-Cr-Cr-Cr})_{0.5}\text{AlC}$  lattices combine the geometrical features of terminal compounds.

### 3.4. Density of Electronic States

The Partial Density of Electronic States (PDOSs) of A, X, and M elements of the first crystal lattice layers of all MAX phases are presented in Figures S5–S13. For parent and terminal Cr- and Fe-based compounds, only Cr or Fe PDOSs are presented, whereas for partially Fe-substituted  $(\text{Fe-Cr-Cr-Cr})_{0.5}\text{AC}$  both Fe and Cr PDOSs of the first and second crystalline layers, respectively, are presented.

The electron densities at the Fermi level for both  $\alpha$  and  $\beta$  electrons of Cr ions in  $\text{Cr}_2\text{GeC}$  are almost identical (Figure S5). Incorporation of Fe ions with consequent formation of  $(\text{Fe-Cr-Cr-Cr})_{0.5}\text{GeC}$  MAX phases (Figure S6) leads to a noticeable polarization at the Fermi level for chromium states combined with a weak one for iron. For Fe in the  $\text{Fe}_2\text{GeC}$  MAX phase, the  $\beta$  electron density at the Fermi level displays higher intensity (Figure S7). In all the germanium-containing phases, carbon has insignificant density around the Fermi level, with higher germanium partial DOSs. In the  $\text{Fe}_2\text{GeC}$  MAX phase, in the range from 0 to  $-1$  eV, carbon has a high overall density coupled with iron states, which may indicate the formation of strong chemical bonds and potentially lead to the formation of an iron carbide phase during the synthesis.

In the silicon-based MAX phases, partial Cr electron density at the Fermi level for  $\alpha$  and  $\beta$  states could be considered as negligibly small (Figure S8). Substitution of Cr ions with consequent formation of  $(\text{Fe-Cr-Cr-Cr})_{0.5}\text{SiC}$  MAX phase (Figure S9) leads to a noticeable polarization of Cr and Fe partial electron densities at the Fermi level. For iron in the  $\text{Fe}_2\text{SiC}$  MAX phase, the polarization is slight (Figure S10). In all silicon-based phases, carbon and silicon have an insignificant density around the Fermi level. For the  $\text{Fe}_2\text{SiC}$  MAX phase in the range from 0 to  $-2$  eV, silicon and carbon have high overall electron density coupled with iron which may be interpreted as a tendency to form silicide and iron

carbide phases. Probably due to the tendency to form silicides of different 3d, 4d and 5d metals, only the Ti-containing silicon MAX phases were detected experimentally.

In aluminum-based MAX phases, Cr partial electron density at the Fermi level for the  $\alpha$  channel is essentially different from the  $\beta$  one. The same spin distribution is observed for aluminum-based compounds (Figure S11). Substitution of Cr ions with the formation of (Fe-Cr-Cr-Cr)<sub>0.5</sub>AlC MAX phase (Figure S12) leads to the absence of noticeable polarization at the Fermi level for all elements. The iron partial density of states in the Fe<sub>2</sub>AlC MAX phase is slightly polarized at the Fermi level (Figure S13). For all aluminum-based MAX phases, carbon atoms demonstrate insignificantly small density of states in the Fermi level region.

### 3.5. Magnetic Properties

The relative energies of all localized spin states (both ferrimagnetic ( $\Delta E_{\text{FiM-FM}}$ ) and antiferromagnetic ( $\Delta E_{\text{AFM-}n\text{-FM}}$ ) with respect to the ferromagnetic ( $E_{\text{FM}}$ ) one) and total spin densities per unit cells for (Cr<sub>3</sub>Fe<sub>1</sub>)<sub>0.5</sub>AC are presented in Table 1. The magnetic moments are specified according to the AFM- $n$  scheme (Table S2). In the process of structural optimization, the direction of the magnetic moments located at metal ions in aluminum-based MAX phases was preserved in contrast to the germanium- and silicon-containing phases, for which the directions are not conserved. It is necessary to note that for substituted lattices with multiple nonequivalent transition metal ions with different spin moments pure antiferromagnetic states cannot be achieved since the moments cannot be mutually compensated.

**Table 1.** Relative energies ( $\Delta E_{\text{FiM-FM}}$ ,  $\Delta E_{\text{AFM-}n\text{-FM}}$ ) with respect to the ferromagnetic state (eV) and total magnetic moments ( $\mu_{\text{B}}$ ) per cell of the (Cr<sub>4-x</sub>Fe<sub>x</sub>)<sub>0.5</sub>AC (A = Ge, Si, Al) MAX phases at different magnetic orders (MO).

MAX Phase	$\Delta E_{\text{FiM-FM}}$	$\Delta E_{\text{AFM-}n\text{-FM}}$	MO	$\mu_{\text{B}}$
Cr <sub>2</sub> GeC	a	a	FM	11.57
(Fe-Cr-Cr-Cr) <sub>0.5</sub> GeC	-0.13 <sup>b</sup>	—	FiM-3	6.09
(Cr-Fe-Cr-Cr) <sub>0.5</sub> GeC	-0.13 <sup>b</sup>	—	FiM-2	6.09
(Cr-Cr-Fe-Cr) <sub>0.5</sub> GeC	-0.13 <sup>b</sup>	—	FiM-4	6.09
(Cr-Cr-Cr-Fe) <sub>0.5</sub> GeC	-0.13 <sup>b</sup>	—	FiM-1	6.09
Fe <sub>2</sub> GeC	-0.10	—	FiM	5.86
Cr <sub>2</sub> SiC	-1.15	-1.39	FiM <sup>c</sup>	1.38
(Fe-Cr-Cr-Cr) <sub>0.5</sub> SiC	0.07	—	FM	9.58
(Cr-Fe-Cr-Cr) <sub>0.5</sub> SiC	-0.01	—	FiM-3	5.1
(Cr-Cr-Fe-Cr) <sub>0.5</sub> SiC	0.02	—	FM	9.6
(Cr-Cr-Cr-Fe) <sub>0.5</sub> SiC	0.19	—	FM	9.61
Fe <sub>2</sub> SiC	0.07	—	FM	6.46
Cr <sub>2</sub> AlC	-0.80	-0.56	FiM	1.8
(Fe-Cr-Cr-Cr) <sub>0.5</sub> AlC	-0.14	-0.20	FiM <sup>d</sup>	-0.42
(Cr-Fe-Cr-Cr) <sub>0.5</sub> AlC	-0.06	-0.14	FiM <sup>d</sup>	0.36
(Cr-Cr-Fe-Cr) <sub>0.5</sub> AlC	-0.08	-0.31	FiM <sup>d</sup>	-1.31
(Cr-Cr-Cr-Fe) <sub>0.5</sub> AlC	-0.02	-0.25	FiM <sup>d</sup>	1.31
Fe <sub>2</sub> AlC	-0.50	-0.28	FiM	3.32

<sup>a</sup> Only FM state. <sup>b</sup> Difference less of 0.001. <sup>c</sup> The magnetic moment direction is formally set according to AFM-3; however, due to the nonequivalent ions in the cell, the system is in the FiM state. <sup>d</sup> The magnetic moment direction is formally set according to AFM-6; however, due to the nonequivalent ions in the cell, the system is in the FiM state.

For the Cr<sub>2</sub>GeC MAX phase (Table 1), the ferromagnetic spin-ordered state is favorable with respect to energy. Electronic structure calculations at the B3LYP level of theory favor the ferromagnetic ordering in a cell over other publications [54,56] where the PBE + U method was used. Considering that the chemical bonding of these compounds is of the mixed covalent ion-metal type, the use of hybrid methods to describe the electronic structure seems preferable. Experimental work [55,57] shows that these materials can have challenging magnetic properties and that doping can lead to ferromagnetism. For substituted MAX phases, different spin-ordered lattices were predetermined for electronic structure calculation (Table S2); however, during the optimization the magnetic moments changed their directions and values and the ferrimagnetic states always appeared favorable with respect to energy. The exception was the Cr<sub>2</sub>GeC MAX phase for which the ground state was detected as ferromagnetic. When one Cr ion is replaced by Fe, the magnetic moment per unit cell decreases because another Cr acquires negative magnetic moment equal to  $-2.70 \mu_B$ . For this reason, all single-substituted structures correspond to a stable ferrimagnetic state. The Fe<sub>2</sub>GeC compound is also a ferrimagnet since one of the Fe ions acquires a negative magnetic moment equal to  $-0.99 \mu_B$  with positive moments for the remaining Fe ions.

The Cr ion in Cr<sub>2</sub>GeC has its own magnetic moment equal to  $3.39 \mu_B$ , which corresponds to the Cr<sup>+3</sup> oxidation state. When one Cr is replaced by Fe, the ferrimagnetic state appears due to the fact that the magnetic moment on one chromium atom is equal to  $-2.70 \mu_B$  (Cr<sup>+3</sup>) and two other Cr<sup>+3</sup> ions bear the moments equal to  $3.43 \mu_B$ . The iron atom has an intrinsic magnetic moment of  $2.69 \mu_B$ , which corresponds to the Fe<sup>+3</sup> oxidation state. In the Fe<sub>2</sub>GeC structure, four iron ions have different magnetic moments, namely  $2.63$ ,  $-0.99$ ,  $1.70$ , and  $2.81 \mu_B$ . This indicates that Fe centers may have different oxidation states (Fe<sup>+2</sup>/Fe<sup>+3</sup>) in one unit cell.

For the (Cr<sub>4-x</sub>Fe<sub>x</sub>)<sub>0.5</sub>SiC MAX phase, the ferromagnetic state prevails over the ferrimagnetic one. Substitution may convert ferrimagnetic spin ordering to ferromagnetic (Table 1). For the Cr<sub>2</sub>SiC MAX phase, the magnetic moment direction was set according to AFM-3 spin ordering and it was conserved during optimization. However, the total magnetic moment per unit cell is high ( $1.38 \mu_B$ ), which is atypical for antiferromagnetic lattices and can be explained by redistribution of the intrinsic magnetic moments over transition metal ions. All four chromium ions have different intrinsic magnetic moments, namely  $3.10$ ,  $2.80$ ,  $-2.90$ , and  $-1.50 \mu_B$ . Obviously, the second and the third layers of chromium ions in the unit cell almost compensate each other, while the main contribution to the total magnetic moment comes from chromium ions in the first and fourth layers with final ferrimagnetic ordering. The values of the intrinsic magnetic moments localized at transition metal ions also indicate that Cr are in different oxidation states:  $3.10$ ,  $2.80$ , and  $-2.90 \mu_B$  for Cr<sup>+3</sup> and  $-1.50 \mu_B$  for Cr<sup>+2</sup>. In the remaining phases, chromium ions are in +3 oxidation state, which is confirmed by the intrinsic magnetic moments close to  $3 \mu_B$  per metal ion. Iron is in +2 oxidation state, except for (Cr-Fe-Cr-Cr)<sub>0.5</sub>SiC where the oxidation state changes for +3 with corresponding  $-2.60 \mu_B$  spin moment. The magnetic moment of  $-2.60 \mu_B$  localized at iron in (Cr-Fe-Cr-Cr)<sub>0.5</sub>SiC causes the ferrimagnetic state (FiM-3) and the lower total magnetic moment of  $5.10 \mu_B$  per MAX phase unit cell as compared with the other substituted (Cr<sub>3</sub>Fe<sub>1</sub>)<sub>0.5</sub>SiC structures. In the Fe<sub>2</sub>SiC structure, all iron ions are in +2 oxidation state with Fe magnetic moment equal to  $1.70 \mu_B$ .

Aluminum-based MAX phases conventionally have lower spin moments as compared with the silicon- and germanium-containing ones, but are more stable [58] and, consequently, more promising for synthesis with substitution of Cr by other transition metals. The true antiferromagnetic states cannot be obtained in a substituted structure though because of the differences between the iron and chromium magnetic moments. In particular, (Fe-Cr-Cr-Cr)<sub>0.5</sub>AlC and (Cr-Fe-Cr-Cr)<sub>0.5</sub>AlC phases have a total magnetic moment of  $0.42 \mu_B$  per unit cell.

The Cr ions in Cr<sub>2</sub>AlC phase are in +3 oxidation state with corresponding magnetic moments equal to  $1.19 \mu_B$ , although, according to [10], the magnetic moment for chromium

is zero, which corresponds to +2 oxidation state. It should be noted that at PBE+U approach should be used for correct reproduction of the spin moments localized at transitional metal ions since the original PBE underestimates the magnetic moments by 30–40% and the +3 oxidation state should be considered. Substitution of Cr by Fe in  $(\text{Fe-Cr-Cr-Cr})_{0.5}\text{AlC}$  and  $(\text{Cr-Fe-Cr-Cr})_{0.5}\text{AlC}$  lattices conserves the chromium oxidation state. In contrast, chromium ions of the third and fourth layers of  $(\text{Cr-Cr-Fe-Cr})_{0.5}\text{AlC}$  and  $(\text{Cr-Cr-Cr-Fe})_{0.5}\text{AlC}$  lattices pass into the +2 oxidation state with Cr spin moments equal to 2.40 and 2.44  $\mu_B$ . The oxidation state of the iron ion in the  $\text{Fe}_2\text{AlC}$  MAX phase is +3, while in the substituted  $(\text{Fe-Cr-Cr-Cr})_{0.5}\text{AlC}$  phase it is equal to +2 ( $\text{Fe} = 2.47\mu_B$ ).

#### 4. Conclusions

Based on electronic structure calculations, it was shown that substitution of Cr ions by Fe ones in  $(\text{Cr}_{4-x}\text{Fe}_x)_{0.5}\text{AC}$  ( $A = \text{Ge, Si, Al}$ ) MAX phases provides stable lattices with the greatest energy stability for single-substituted compounds with visible reduction of crystal lattice parameters. Band structure and DOS diagrams showed that all MAX phases demonstrate metallic conductivity with high electronic density at the Fermi level.  $(\text{Cr}_{4-x}\text{Fe}_x)_{0.5}\text{GeC}$  MAX phases exhibit a gradual appearance of van Hove singularity upon increasing Fe content. The  $\text{Cr}_2\text{AlC}$  MAX phase clearly demonstrates the Dirac cone in the band structure in contrast with germanium- and silicon-based compounds, which can lead to the formation of topological phases and significantly affect their transport properties. At the B3LYP level of theory, the ferro- and ferrimagnetic spin orderings in partially substituted MAX phases are favorable with respect to energy.  $\text{Cr}_2\text{SiC}$ -to- $\text{Fe}_2\text{SiC}$  and  $\text{Cr}_2\text{GeC}$ -to- $\text{Fe}_2\text{GeC}$  structural transformations led to a change in the magnetic states, while for  $\text{Cr}_2\text{AlC}$ - $\text{Fe}_2\text{AlC}$  the FiM spin order was preserved. In the last case, the difference between the spin states is minor, which may open up the prospect of using these structures in spintronic devices. It was shown that single-substituted  $(\text{Cr}_3\text{Fe}_1)_{0.5}\text{AC}$  ( $A = \text{Ge, Si, Al}$ ) MAX phases could be very beneficial for multiple spin-related applications.

**Supplementary Materials:** The following supporting information can be downloaded at: <https://www.mdpi.com/article/10.3390/magnetochemistry9060147/s1>, Table S1. Atomic and ionic radii\* [59]; Table S2. Schematic of the ferromagnetic (FM), ferrimagnetic (FiM- $n$ ), and antiferromagnetic (AFM- $n$ ) ordering of the Cr and Fe magnetic moments in the  $(\text{Cr-Fe-Cr-Cr})_{0.5}\text{SiC}$  structure. Green and red arrows indicate the spins up and spin down directions on M atoms, respectively; Figure S1. Comparison of unit cell parameters  $a$ ,  $b$  (on the left), and  $c$  (on the right) obtained using different functionals; Figure S2. Iron and chromium partial charges in the  $\text{CrFeSiC}$  structure obtained using different functionals (up) and magnetic moment  $\text{Satom}$  ( $\mu_B$ ) of nonequivalent atoms of the metals. Iron and chromium magnetic moments in the  $\text{CrFeSiC}$  structure obtained using different functionals (down); Figure S3. Brillouin zone of a hexagonal lattice; Figure S4. Binding energy change in the  $(\text{Cr}_{4-x}\text{Fe}_x)_{0.5}\text{AC}$  ( $A = \text{Ge, Si, Al}$ ) crystal lattices in the ferromagnetic state upon substitution of Fe atoms for Cr ones. Blue, orange, and gray histograms correspond to the phases with Ge, Si, and Al as the A element; Figure S5. Densities of states of the  $\text{Cr}_2\text{GeC}$ . Partial densities of states of the M element of the first crystal lattice layer (blue), of the M element of the second crystal lattice layer (lilac), of the A element (dark blue), and of the element  $X = \text{C}$  (burgundy); Figure S6. Densities of states of the  $(\text{Cr-Fe-Cr-Cr})\text{GeC}$ ; Figure S7. Densities of states of the  $\text{Fe}_2\text{GeC}$ ; Figure S8. Densities of states of the  $\text{Cr}_2\text{SiC}$ ; Figure S9. Densities of states of the  $(\text{Cr-Fe-Cr-Cr})\text{SiC}$ ; Figure S10. Densities of states of the  $\text{Fe}_2\text{SiC}$ ; Figure S11. Densities of states of the  $\text{Cr}_2\text{AlC}$ ; Figure S12. Densities of states of the  $(\text{Cr-Fe-Cr-Cr})\text{AlC}$ ; Figure S13. Densities of states of the  $\text{Fe}_2\text{AlC}$ .

**Author Contributions:** Conceptualization, J.S.O., A.S.T., S.N.V., S.G.O., P.V.A. and F.N.T.; Data curation, A.S.T., S.N.V. and S.G.O.; Funding acquisition, S.N.V. and S.G.O.; Investigation, A.V.K., N.A.F., D.A.I., V.V.K., A.A.S., E.M.M., O.A.M. and F.N.T.; Methodology, A.A.S. and F.N.T.; Project administration, S.N.V.; Supervision, S.N.V. and F.N.T.; Visualization, J.S.O., A.A.S. and F.N.T.; Writing—original draft, A.V.K., J.S.O., N.A.F., A.A.S., A.S.T. and F.N.T.; Writing—review & editing, P.V.A. and F.N.T. All authors have read and agreed to the published version of the manuscript.

**Funding:** This study was supported by the Russian Science Foundation, project no. 21-12-00226. P.V.A. acknowledges the support of the National Research Foundation of the Republic of Korea, grant no. NRF 2021R1A2C1010455.

**Institutional Review Board Statement:** Not applicable.

**Informed Consent Statement:** Not applicable.

**Data Availability Statement:** The data that support the findings of this study are available upon reasonable request from the authors.

**Acknowledgments:** The authors thank the Joint Supercomputer Center (JSCC) of the Russian Academy of Sciences and laboratory of Magnetic MAX Materials for providing molecular simulation.

**Conflicts of Interest:** The authors declare no conflict of interest.

## References

1. Smetkin, A.; Maiorova, I. Properties of materials based on the MAX-phases (Review). *PNIPU Bull. Mech. Eng. Mater. Sci.* **2015**, *17*, 120–138. [[CrossRef](#)]
2. Zhang, Z.; Duan, X.; Jia, D.; Zhou, Y.; van der Zwaag, S. On the formation mechanisms and properties of MAX phases: A review. *J. Eur. Ceram. Soc.* **2021**, *41*, 3851–3878. [[CrossRef](#)]
3. Sui, J.; Liu, D.; Wang, C.; Wang, L.; Zhong, B.; Ma, Y. MAX phase-derived woolen ball-like  $K_2Ti_8O_{17}$  with excellent surface-enhanced Raman scattering property. *Ceram. Int.* **2023**, *49*, 15145–15153. [[CrossRef](#)]
4. Yuan, J.; Wang, Z.; Ma, G.; Bai, X.; Li, Y.; Cheng, X.; Ke, P.; Wang, A. MAX phase forming mechanism of M–Al–C (M = Ti, V, Cr) coatings: In-situ X-ray diffraction and first-principle calculations. *J. Mater. Sci. Technol.* **2023**, *143*, 140–152. [[CrossRef](#)]
5. Thorsteinsson, E.B.; Ingason, A.S.; Magnus, F. Magnetic ordering and magnetocrystalline anisotropy in epitaxial  $Mn_2GaC$  MAX phase thin films. *Phys. Rev. Mater.* **2023**, *7*, 34409. [[CrossRef](#)]
6. Hamm, C.M.; Bocarsly, J.D.; Seward, G.; Kramm, U.I.; Birkel, C.S. Non-conventional synthesis and magnetic properties of MAX phases  $(Cr/Mn)_2AlC$  and  $(Cr/Fe)_2AlC$ . *J. Mater. Chem. C* **2017**, *5*, 5700–5708. [[CrossRef](#)]
7. Pinek, D.; Ito, T.; Ikemoto, M.; Yaji, K.; Nakatake, M.; Shin, S.; Ouisse, T. Unified description of the electronic structure of M2AC nanolamellar carbides. *Phys. Rev. B* **2019**, *100*, 75144. [[CrossRef](#)]
8. 15 Years of Graphene Electronics. *Nat. Electron.* **2019**, *2*, 369. [[CrossRef](#)]
9. Goossens, N.; Tunca, B.; Lapauw, T.; Lambrinou, K.; Vleugels, J. *MAX Phases, Structure, Processing, and Properties*; Elsevier: Amsterdam, The Netherlands, 2021.
10. Dahlqvist, M.; Alling, B.; Abrikosov, I.A.; Rosén, J. Magnetic nanoscale laminates with tunable exchange coupling from first principles. *Phys. Rev. B—Condens. Matter Mater. Phys.* **2011**, *84*, 220403. [[CrossRef](#)]
11. Dahlqvist, M.; Rosén, J. Predictive theoretical screening of phase stability for chemical order and disorder in quaternary 312 and 413 MAX phases. *Nanoscale* **2020**, *12*, 785–794. [[CrossRef](#)]
12. Mockute, A.; Dahlqvist, M.; Emmerlich, J.; Hultman, L.; Schneider, J.M.; Persson, P.O.Å.; Rosén, J. Synthesis and ab initio calculations of nanolaminated  $(Cr,Mn)_2AlC$  compounds. *Phys. Rev. B* **2013**, *87*, 94113. [[CrossRef](#)]
13. Salikhov, R.; Semisalova, A.S.; Petruhins, A.; Ingason, Á.S.; Rosén, J.; Wiedwald, U.; Farle, M. Magnetic anisotropy in the  $(Cr_{0.5}Mn_{0.5})_2GaC$  MAX phase. *Mater. Res. Lett.* **2015**, *3*, 156–160. [[CrossRef](#)]
14. Salikhov, R.; Meshkian, R.; Weller, D.; Zingsem, B.; Spoddig, D.; Lu, J.; Ingason, Á.S.; Zhang, H.; Rosén, J.; Wiedwald, U.; et al. Magnetic properties of nanolaminated  $(Mo_{0.5}Mn_{0.5})_2GaC$  MAX phase. *J. Appl. Phys.* **2017**, *121*, 163904. [[CrossRef](#)]
15. Ohmer, D.; Opahle, I.; Singh, H.K.; Zhang, H. Stability predictions of magnetic M2AX compounds. *J. Phys. Condens. Matter* **2019**, *31*, 405902. [[CrossRef](#)] [[PubMed](#)]
16. Tao, Q.; Lu, J.; Dahlqvist, M.; Mockute, A.; Calder, S.; Petruhins, A.; Meshkian, R.; Rivin, O.; Potashnikov, D.; Caspi, E.N.; et al. Atomically Layered and Ordered Rare-Earth i -MAX Phases: A New Class of Magnetic Quaternary Compounds. *Chem. Mater.* **2019**, *31*, 2476–2485. [[CrossRef](#)]
17. Petruhins, A.; Ingason, Á.S.; Lu, J.; Magnus, F.; Olafsson, S.; Rosén, J. Synthesis and characterization of magnetic  $(Cr_{0.5}Mn_{0.5})_2GaC$  thin films. *J. Mater. Sci.* **2015**, *50*, 4495–4502. [[CrossRef](#)]
18. Novoselova, I.P.; Petruhins, A.; Wiedwald, U.; Weller, D.; Rosén, J.; Farle, M.; Salikhov, R. Long-term stability and thickness dependence of magnetism in thin  $(Cr_{0.5}Mn_{0.5})_2GaC$  MAX phase films. *Mater. Res. Lett.* **2019**, *7*, 159–163. [[CrossRef](#)]
19. Novoselova, I.P.; Petruhins, A.; Wiedwald, U.; Ingason, Á.S.; Hase, T.; Magnus, F.; Kapaklis, V.; Palisaitis, J.; Spasova, M.; Farle, M.; et al. Large uniaxial magnetostriction with sign inversion at the first order phase transition in the nanolaminated  $Mn_2GaC$  MAX phase. *Sci. Rep.* **2018**, *8*, 2637. [[CrossRef](#)]
20. Lyaschenko, S.; Maximova, O.; Shevtsov, D.; Varnakov, S.; Tarasov, I.; Wiedwald, U.; Rosén, J.; Ovchinnikov, S.G.; Farle, M. Optical and magneto-optical properties of epitaxial  $Mn_2GaC$  MAX phase thin film. *J. Magn. Magn. Mater.* **2021**, *528*, 167803. [[CrossRef](#)]
21. Nowotny, H. Strukturchemie einiger Verbindungen der Übergangsmetalle mit den elementen C, Si, Ge, Sn. *Prog. Solid State Chem.* **1971**, *5*, 27–70. [[CrossRef](#)]

22. Ingason, Á.S.; Mockute, A.; Dahlqvist, M.; Magnus, F.; Olafsson, S.; Arnalds, U.B.; Alling, B.; Abrikosov, I.A.; Hjörvarsson, B.; Persson, P.O.Å.; et al. Magnetic Self-Organized Atomic Laminate from First Principles and Thin Film Synthesis. *Phys. Rev. Lett.* **2013**, *110*, 195502. [CrossRef]
23. Eklund, P.; Bugnet, M.; Mauchamp, V.; Dubois, S.; Tromas, C.; Jensen, J.; Piroux, L.; Gence, L.; Jaouen, M.; Cabioch, T. Epitaxial growth and electrical transport properties of Cr<sub>2</sub>GeC thin films. *Phys. Rev. B* **2011**, *84*, 75424. [CrossRef]
24. Ying, G.; He, X.; Li, M.; Han, W.; He, F.; Du, S. Synthesis and mechanical properties of high-purity Cr<sub>2</sub>AlC ceramic. *Mater. Sci. Eng. A* **2011**, *528*, 2635–2640. [CrossRef]
25. Xiao, L.; Li, S.; Song, G.; Sloof, W.G. Synthesis and thermal stability of Cr<sub>2</sub>AlC. *J. Eur. Ceram. Soc.* **2011**, *31*, 1497–1502. [CrossRef]
26. Ramzan, M.; Lebègue, S.; Ahuja, R. Electronic and mechanical properties of Cr<sub>2</sub>GeC with hybrid functional and correlation effects. *Solid State Commun.* **2012**, *152*, 1147–1149. [CrossRef]
27. Perdew, J.P.; Burke, K.; Ernzerhof, M. Generalized Gradient Approximation Made Simple. *Phys. Rev. Lett.* **1996**, *77*, 3865–3868. [CrossRef]
28. Anisimov, V.I.; Aryasetiawan, F.; Lichtenstein, A.I. First-principles calculations of the electronic structure and spectra of strongly correlated systems: The LDA + U method. *J. Phys. Condens. Matter* **1997**, *9*, 767–808. [CrossRef]
29. Heyd, J.; Scuseria, G.E.; Ernzerhof, M. Hybrid functionals based on a screened Coulomb potential. *J. Chem. Phys.* **2003**, *118*, 8207, Erratum in *J. Chem. Phys.* **2006**, *124*, 219906. [CrossRef]
30. Guido, C.A.; Brémond, E.; Adamo, C.; Cortona, P. Communication: One third: A new recipe for the PBE0 paradigm. *J. Chem. Phys.* **2013**, *138*, 21104. [CrossRef]
31. Becke, A.D. Density-functional thermochemistry. III. The role of exact exchange. *J. Chem. Phys.* **1993**, *98*, 5648–5652. [CrossRef]
32. Lee, C.; Yang, W.; Parr, R.G. Development of the Colle-Salvetti correlation-energy formula into a functional of the electron density. *Phys. Rev. B* **1988**, *37*, 785–789. [CrossRef]
33. Zhao, Y.; Truhlar, D.G. The M06 suite of density functionals for main group thermochemistry, thermochemical kinetics, noncovalent interactions, excited states, and transition elements: Two new functionals and systematic testing of four M06-class functionals and 12 other functionals. *Theor. Chem. Acc.* **2008**, *120*, 215–241. [CrossRef]
34. Zhao, Y.; Truhlar, D.G. A new local density functional for main-group thermochemistry, transition metal bonding, thermochemical kinetics, and noncovalent interactions. *J. Chem. Phys.* **2006**, *125*, 194101. [CrossRef] [PubMed]
35. Vilela Oliveira, D.; Laun, J.; Peintinger, M.F.; Bredow, T. BSSE-correction scheme for consistent gaussian basis sets of double- and triple-zeta valence with polarization quality for solid-state calculations. *J. Comput. Chem.* **2019**, *40*, 2364–2376. [CrossRef] [PubMed]
36. Liao, T.; Wang, J.; Zhou, Y. Chemical bonding and mechanical properties of M<sub>2</sub>AC (M = Ti, V, Cr, A = Al, Si, P, S) ceramics from first-principles investigations. *J. Mater. Res.* **2009**, *24*, 556–564. [CrossRef]
37. Metadger, N.; Beldi, L.; Bouhafs, B.; Ruterana, P. Electronic and magnetic properties of Fe<sub>2</sub>SiC. *Eur. Phys. J. B* **2014**, *87*, 240. [CrossRef]
38. Piskunov, S.; Heifets, E.; Eglitis, R.I.; Borstel, G. Bulk properties and electronic structure of SrTiO<sub>3</sub>, BaTiO<sub>3</sub>, PbTiO<sub>3</sub> perovskites: An ab initio HF/DFT study. *Comput. Mater. Sci.* **2004**, *29*, 165–178. [CrossRef]
39. Ladik, J.; Bogar, F.; Penke, B. Comparison of HF, HF + MP2, LDA, BLYP, and B3LYP band structures of the homopolypeptides. *Int. J. Quantum Chem.* **2004**, *98*, 522–527. [CrossRef]
40. Dovesi, R.; Erba, A.; Orlando, R.; Zicovich-Wilson, C.M.; Civalieri, B.; Maschio, L.; Rérat, M.; Casassa, S.; Baima, J.; Salustro, S.; et al. Quantum-mechanical condensed matter simulations with CRYSTAL. *WIREs Comput. Mol. Sci.* **2018**, *8*, e1360. [CrossRef]
41. Dovesi, R.; Saunders, V.R.; Roetti, C.; Orlando, R.; Pascale, F.; Civalieri, B.; Doll, K.; Harrison, N.M.; Bush, I.J.; Arco, P.D.; et al. User's Manual. 2017. Available online: <http://www.crystal.unito.it/Manuals/crystal17.pdf> (accessed on 20 April 2023).
42. Monkhorst, H.J.; Pack, J.D. Special points for Brillouin-zone integrations. *Phys. Rev. B* **1976**, *13*, 5188–5192. [CrossRef]
43. Gilat, G.; Raubenheimer, L.J. Accurate Numerical Method for Calculating Frequency-Distribution Functions in Solids. *Phys. Rev.* **1966**, *144*, 390–395. [CrossRef]
44. Civalieri, B.; D'Arco, P.; Orlando, R.; Saunders, V.R.; Dovesi, R. Hartree–Fock geometry optimisation of periodic systems with the Crystal code. *Chem. Phys. Lett.* **2001**, *348*, 131–138. [CrossRef]
45. Ghebouli, M.A.; Ghebouli, B.; Fatmi, M.; Bouhemadou, A. Theoretical prediction of the structural, elastic, electronic and thermal properties of the MAX phases X<sub>2</sub>SiC (X = Ti and Cr). *Intermetallics* **2011**, *19*, 1936–1942. [CrossRef]
46. Tomilin, F.N.; Shubin, A.A.; Kozak, V.V.; Ivanova, D.A.; Fedorova, N.A.; Ol'shevskaya, Y.S.; Kovaleva, A.V.; Avramov, P.V.; Ovchinnikov, S.G. Effect of Substitution on Magnetic Moments of Iron and Chromium Atoms in MAX Phases of Type (Cr<sub>4-x</sub>Fe<sub>x</sub>)<sub>0.5</sub>SiC: Theoretical Calculation. *Phys. Met. Metallogr.* **2022**, *123*, 640–644. [CrossRef]
47. Pazniak, A.; Stevens, M.; Dahlqvist, M.; Zingsem, B.; Kibkalo, L.; Felek, M.; Varnakov, S.; Farle, M.; Rosén, J.; Wiedwald, U. Phase Stability of Nanolaminated Epitaxial (Cr<sub>1-x</sub>Fe<sub>x</sub>)<sub>2</sub> AlC MAX Phase Thin Films on MgO(111) and Al<sub>2</sub>O<sub>3</sub> (0001) for Use as Conductive Coatings. *ACS Appl. Nano Mater.* **2021**, *4*, 13761–13770. [CrossRef]
48. Setyawan, W.; Curtarolo, S. High-throughput electronic band structure calculations: Challenges and tools. *Comput. Mater. Sci.* **2010**, *49*, 299–312. [CrossRef]
49. Klein, A.; Jaegermann, W. Review—Electronic Properties of 2D Layered Chalcogenide Surfaces and Interfaces grown by (quasi) van der Waals Epitaxy. *ECS J. Solid State Sci. Technol.* **2020**, *9*, 93012. [CrossRef]

50. Begunovich, L.V.; Kuklin, A.V.; Visotin, M.A.; Kuzubov, A.A.; Tomilin, F.N.; Tarasov, A.S.; Mikhalev, Y.G.; Avramov, P.V. Triple VTe<sub>2</sub>/graphene/VTe<sub>2</sub> heterostructures as perspective magnetic tunnel junctions. *Appl. Surf. Sci.* **2020**, *510*, 145315. [[CrossRef](#)]
51. Yan, W.; Txoperena, O.; Llopis, R.; Dery, H.; Hueso, L.E.; Casanova, F. A two-dimensional spin field-effect switch. *Nat. Commun.* **2016**, *7*, 13372. [[CrossRef](#)]
52. Alymov, G.; Vyurkov, V.; Ryzhii, V.; Svintsov, D. Abrupt current switching in graphene bilayer tunnel transistors enabled by van Hove singularities. *Sci. Rep.* **2016**, *6*, 24654. [[CrossRef](#)]
53. Flatten, T.; Matthes, F.; Petruhins, A.; Salikhov, R.; Wiedwald, U.; Farle, M.; Rosén, J.; Bürgler, D.E.; Schneider, C.M. Direct measurement of anisotropic conductivity in a nanolaminated (Mn<sub>0.5</sub>Cr<sub>0.5</sub>)<sub>2</sub>GaC thin film. *Appl. Phys. Lett.* **2019**, *115*, 94101. [[CrossRef](#)]
54. Mattesini, M.; Magnuson, M. Electronic correlation effects in the Cr<sub>2</sub>GeC M<sub>n+1</sub>AX<sub>n</sub> phase. *J. Phys. Condens. Matter* **2013**, *25*, 35601. [[CrossRef](#)]
55. Magnuson, M.; Mattesini, M. Magnetic anisotropy in Cr<sub>2</sub>GeC investigated by X-ray magnetic circular dichroism and ab initio calculations. *J. Magn. Magn. Mater.* **2020**, *501*, 166470. [[CrossRef](#)]
56. Benouis, M.; Azzaz, Y.; Ameri, M.; Arbouche, O.; Bennadji, A.; Bensaid, D.; Al-Douri, Y. Electronic and Magnetic Properties of Cr<sub>2</sub>GeC with GGA + U Approximation. *J. Supercond. Nov. Magn.* **2016**, *29*, 1267–1272. [[CrossRef](#)]
57. Liu, Z.; Waki, T.; Tabata, Y.; Nakamura, H. Mn-doping-induced itinerant-electron ferromagnetism in Cr<sub>2</sub>GeC. *Phys. Rev. B—Condens. Matter Mater. Phys.* **2014**, *89*, 54435. [[CrossRef](#)]
58. Dahlgvist, M.; Rosén, J. The rise of MAX phase alloys—Large-scale theoretical screening for the prediction of chemical order and disorder. *Nanoscale* **2022**, *14*, 10958–10971. [[CrossRef](#)]
59. Emsley, J. *The Elements*, 3rd ed.; Oxford University Press: Oxford, UK, 1989; p. 264.

**Disclaimer/Publisher’s Note:** The statements, opinions and data contained in all publications are solely those of the individual author(s) and contributor(s) and not of MDPI and/or the editor(s). MDPI and/or the editor(s) disclaim responsibility for any injury to people or property resulting from any ideas, methods, instructions or products referred to in the content.